Mechanism of proton-coupled electron transfer described with QM/MM implementation of coupled-perturbed density-functional tight-binding

Denis Maag, Josua Böser, Henryk A. Witek, et al.

COLLECTIONS

Paper published as part of the special topic on Modern Semiempirical Electronic Structure Methods

View Online

Export Citation

CrossMark

ARTICLES YOU MAY BE INTERESTED IN

AIP Publishing

Mechanism of proton-coupled electron transfer described with QM/MM implementation of coupled-perturbed density-functional tight-binding

Denis Maag,[1] [ID] Josua Böser,[1] [ID] Henryk A. Witek,[2,3] [ID] Ben Hourahine,[4] [ID] Marcus Elstner,[1,5] [ID]
and Tomáš Kubař[1,a)] [ID]

AFFILIATIONS

[1] Institute of Physical Chemistry, Karlsruhe Institute of Technology, 76131 Karlsruhe, Germany
[2] Department of Applied Chemistry and Institute of Molecular Science, National Yang Ming Chiao Tung University,
  Hsinchu, Taiwan
[3] Center for Emergent Functional Matter Science, National Yang Ming Chiao Tung University, Hsinchu, Taiwan
[4] Department of Physics, University of Strathclyde, Glasgow G4 0NG, United Kingdom
[5] Institute of Biological Interfaces (IBG-2), Karlsruhe Institute of Technology, 76131 Karlsruhe, Germany

Note: This paper is part of the JCP Special Topic on Modern Semiempirical Electronic Structure Methods.
[a)]Author to whom correspondence should be addressed: tomas.kubar@kit.edu

ABSTRACT

Coupled-perturbed equations for degenerate orbitals were implemented for third order density-functional tight binding, which allowed the use of Mulliken charges as reaction coordinates. The method was applied to proton-coupled electron transfer (PCET) reactions in a model system and thoroughly tested for QM and QM/MM setups (i.e., coupled quantum and molecular mechanics). The performed enhanced sampling simulations were stable, and the obtained potentials of the mean force were able to address the thermodynamic and kinetic features of the reactions by showing the expected topography and energy barriers. Hence, this method has the potential to distinguish between concerted and sequential mechanisms and could next be applied to proton-coupled electron transfer reactions in more complex systems like proteins.

I. INTRODUCTION

In numerous biological processes, a proton transfer is coupled to an electron transfer in a so-called proton-coupled electron transfer (PCET) reaction, which can occur in a sequential or concerted manner.[1,2] The sequential pathway can proceed via two mechanisms: first, an electron transfer (ET) followed by a proton transfer (PT) or a PT followed by an ET. In the concerted proton–electron transfer, both transitions occur in one step. The time scales of ET and PT depend significantly on the transfer distance and on the environment, e.g., water or protein.

A prime example of PCET reactions in a protein is the reduction of ribonucleotides by the enzyme ribonucleotide reductase (RNR).[3,4] The catalytic reaction features a long-range ET over ~32 Å via several PCETs along a pathway of redox-active amino acids. Most of the involved amino acids are tyrosines of which one (Y731) has to dynamically rearrange in order to facilitate the ET and PT.[5] Thus, conformational changes are of great importance for the correct description of PCETs.

PCET reactions have been extensively studied over recent decades, and dedicated simulation protocols have been developed, such as those by Cukier[6–8] and Hammes-Schiffer et al.[9–11] The

general goal of all these methods is to obtain the correct reaction energy profiles of the studied systems. The variety of available methods and their applications were described in several recent reviews and perspectives.[12–18]

We introduced a new concept of free energy calculations, in which Mulliken charges from the density-functional tight binding (DFTB) method are used to construct reaction coordinates in biasing potential simulations.[19] The method performs very well for systems that are described by DFTB completely; however, it fails to describe QM/MM systems accurately. We demonstrated that this is due to the missing derivatives of QM charges with respect to coordinates of MM atoms. Another minor issue is that so far the method has only considered second-order DFTB (DFTB2), while the third-order DFTB expansion (DFTB3) may be desirable for the description of anionic species.

In this work, we derive and implement the necessary additional derivatives in order to perform free energy calculations using reaction coordinates containing QM charges in a hybrid QM/MM setup. Additionally, the calculation of the derivative of atomic Hamiltonian shifts (see below) in the CP equations is extended to comply with the DFTB3 formalism. To test the implementation thoroughly, we performed QM and QM/MM metadynamics of PCET reactions taking place between two tyrosine sidechains, considering 32 situations that differ in the charge state, orientation of the sidechains, and environment. The insight obtained from the resulting potentials of mean force (PMFs) will be discussed.

II. METHODS

A. External biasing potential involving atomic charges

Our previously introduced concept of free energy calculations uses net Mulliken charges, Δq,[20] in the density-functional tight binding (DFTB) method as one or more collective variables S,

$$S = S(\Delta q) = S(\Delta q(\vec{r})), \tag{1}$$

in biasing potential simulations, such as metadynamics or umbrella sampling.[19] The atomic charges Δq are readily available in DFTB and depend on molecular geometry, i.e., the atomic positions $\vec{r}$. The forces on atoms due to an applied biasing potential $V(S)$ are obtained as the derivatives of the biasing potential with respect to atomic coordinates a. By the chain rule, this leads to

$$F_a = \frac{\partial V(S(\Delta q(\vec{r})))}{\partial a} = \frac{dV(S)}{dS} \cdot \frac{dS(\Delta q)}{d\Delta q} \cdot \frac{\partial \Delta q(\vec{r})}{\partial a}. \tag{2}$$

Since V is usually a quadratic function or the sum of Gaussian functions, the first derivative $dV(S)/dS$ is easily calculated, as is the derivative of the reaction coordinate $dS(Q)/dQ$. The derivatives of atomic charges with respect to atomic coordinates $\partial Q(\vec{r})/\partial a$ have to be calculated by means of coupled-perturbed (CP) equations, which were originally derived, implemented, and tested by Witek *et al.*[21]

B. Density-functional tight-binding

DFT is significantly faster than *ab initio* quantum chemical methods; however, it is still limited to small system sizes (~100

atoms) and sub-nanosecond ranges of molecular dynamics (MD) simulations. Larger system sizes and longer temporal scales are accessible with semiempirical (SE) methods such as the density-functional tight-binding (DFTB) method, which is based on DFT and introduces certain well-controlled approximations and element-specific parameters.

The starting point of the development of DFTB is the DFT total energy, which is expanded in a Taylor series in terms of electron density and expressed as the sum of a suitable reference density (a superposition of neutral atomic densities) and a density fluctuation. The DFTB total energy is obtained by such an expansion of the exchange–correlation energy functional in a Taylor series and by removing the constant double-counting intra-atomic energy contributions from each atom at the reference density.[22–24] The DFTB3 method is obtained by truncating the Taylor series at the third order.[25,26]

Only the valence electrons are explicitly considered, and the Kohn–Sham orbitals are expanded in a minimal basis,

$$\Psi_i = \sum_\mu c_{\mu i} \phi_\mu, \tag{3}$$

with only one radial function for each angular momentum state. The basis functions ϕ_μ are obtained from DFT calculations with an additional confinement potential, which makes the orbitals more compact. The density fluctuations in the second- and third-order terms are expressed as a sum of spherically symmetric atomic contributions. These are represented by net atomic Mulliken charges Δq_A, obtained by subtracting the number of electrons of a neutral atom q_A^0 from the gross atomic charges q_A,

$$\Delta q_A = q_A - q_A^0, \tag{4}$$

resulting from the Mulliken analysis

$$q_A = \sum_i^{\text{occ}} n_i \sum_{\mu \in A} \sum_B \sum_{v \in B} c_\mu^i c_v^i S_{\mu v}. \tag{5}$$

The final DFTB3 energy expression then reads

$$E^{\text{DFTB3}} = \frac{1}{2} \sum_{A,B} V_{AB}^{\text{rep}} + \sum_i^{\text{occ}} \sum_{\mu \in A} \sum_{v \in B} c_\mu^i c_v^i H_{\mu v}^0$$
$$+ \frac{1}{2} \sum_{A,B} \gamma_{AB} \Delta q_A \Delta q_B + \frac{1}{3} \sum_{A,B} (\Delta q_A)^2 \Delta q_B \Gamma_{AB}. \tag{6}$$

Here, the two-body repulsive potentials V_{AB}^{rep} are functions of interatomic distances A–B, represented by splines specific to pairs of chemical elements A, B. The Hamiltonian $H_{\mu v}^0$ and overlap $S_{\mu v}$ matrix elements are precomputed and tabulated for each pair of orbitals and interpolated for a given geometry during a DFTB calculation. $\{n_i\}$ are the molecular orbital occupations. The analytical function γ_{AB} of interatomic distance A–B describes the Coulombic interaction of atomic charge densities and involves the atomic Hubbard parameters U_A, related to chemical hardnesses. The function Γ_{AB} is the charge derivative of γ_{AB} and includes the charge derivative of the Hubbard parameter, U_A^d.

The minimum energy is obtained with the variation principle, leading to

$$\sum_v c_v^i (H_{\mu v} - \varepsilon_i S_{\mu v}) = 0. \tag{7}$$

The charge-dependent Hamiltonian $H_{\mu v}$ is given as

$$H_{\mu v} = H_{\mu v}^0 + S_{\mu v} \cdot \Omega_{AB}, \tag{8}$$

$$\Omega_{AB} = \sum_C \Delta q_C \left(\frac{\gamma_{AC} + \gamma_{BC}}{2} + \frac{\Delta q_A \Gamma_{AC} + \Delta q_B \Gamma_{BC}}{3} + \frac{\Delta q_C (\Gamma_{CA} + \Gamma_{CB})}{6} \right), \tag{9}$$

where Ω_{AB} is the Hamiltonian shift due to the induced charges. Since the Hamiltonian depends on the Mulliken charges, which in turn depend on the molecular orbital coefficients c_μ^i, Eqs (7) and (8) have to be solved iteratively until self-consistency is reached.

C. Coupled-perturbed DFTB

A recent extension to DFTB is the coupled-perturbed (CP) equations, which calculate the derivative of atomic charges with respect to atomic coordinates. They were first derived and implemented for DFTB2 by Witek *et al.*[21] and later extended to DFTB3 by Hourahine.[27] The CP-DFTB equations must be solved iteratively until self-consistency because they include three sets of quantities that depend on each other.

First, the derivatives of the MO coefficients with respect to the atomic coordinates a are expressed by means of a matrix $\mathscr{U}^{(a)}$,

$$\frac{\partial c_\mu^i}{\partial a} = \sum_m^{MO} U_{mi}^{(a)} c_{\mu m}, \tag{10}$$

where the diagonal elements are obtained as

$$U_{ii}^{(a)} = -\frac{1}{2} \sum_{\mu v}^{AO} c_{\mu i} c_{vi} \frac{\partial S_{\mu v}}{\partial a} \tag{11}$$

and the off-diagonal elements as

$$U_{ij}^{(a)} = \frac{1}{\varepsilon_j - \varepsilon_i} \sum_{M,N}^{atoms} \sum_{\mu \in M} \sum_{v \in N} c_{\mu i} c_{vj}$$
$$\times \left(\frac{\partial H_{\mu v}^0}{\partial a} + \frac{\partial S_{\mu v}}{\partial a}(\Omega_{MN} - \varepsilon_j) + S_{\mu v} \frac{\partial \Omega_{MN}}{\partial a} \right). \tag{12}$$

A good starting point for the iterative CP-DFTB calculation may be the entire matrix $\mathscr{U}^{(a)}$ zeroed.

Second, the derivatives of atomic charges with respect to atomic coordinates are calculated,

$$\frac{\partial \Delta q_A}{\partial a} = \sum_i^{MO} n_i \sum_{\mu \in A}^{AO} \sum_v \left(c_{\mu i} c_{vi} \frac{\partial S_{\mu v}}{\partial a} \right.$$
$$\left. + \sum_m^{MO} \left(U_{mi}^{(a)} (c_{\mu m} c_{vi} + c_{\mu i} c_{vm}) S_{\mu v} \right) \right). \tag{13}$$

Third, the derivative of the atomic shift with respect to atomic coordinates is

$$\frac{\partial \Omega_{AB}}{\partial a} = \frac{1}{2} \sum_C^{QM\,at.} \left(\left(\frac{\partial \gamma_{AC}}{\partial a} + \frac{\partial \gamma_{BC}}{\partial a} \right) \Delta q_C + (\gamma_{AC} + \gamma_{BC}) \frac{\partial \Delta q_C}{\partial a} \right)$$
$$+ \frac{1}{3} \sum_C^{QM\,at.} \left(\Delta q_A \Gamma_{AC} + \Delta q_B \Gamma_{BC} + \Delta q_C \frac{\Gamma_{CA} + \Gamma_{CB}}{2} \right) \frac{\partial \Delta q_C}{\partial a}$$
$$+ \frac{1}{3} \sum_C^{QM\,at.} \left(\frac{\partial \Delta q_A}{\partial a} \Gamma_{AC} + \frac{\partial \Delta q_B}{\partial a} \Gamma_{BC} + \Delta q_A \frac{\partial \Gamma_{AC}}{\partial a} + \Delta q_B \frac{\partial \Gamma_{BC}}{\partial a} \right.$$
$$+ \frac{\partial \Delta q_C}{\partial a} (\Gamma_{CA} + \Gamma_{CB}) + \frac{1}{2} \Delta q_C \left(\frac{\partial \Gamma_{CA}}{\partial a} + \frac{\partial \Gamma_{CB}}{\partial a} \right) \right) \Delta q_C. \tag{14}$$

Then, the resulting $\frac{\partial \Omega_{AB}}{\partial a}$ is cast into Eq. (12), and the procedure continues with the calculation of the matrix $\mathscr{U}^{(a)}$.

D. Additional CP-DFTB equations—dependence on MM coordinates

In the framework of DFTB, the MM region in QM/MM simulations comes into play via the electrostatic potentials Φ_A and Φ_B, induced by all of the involved MM atoms at the QM atoms A and B, respectively. These are added to the atomic Hamiltonian shift from Eq. (9),

$$\Omega_{AB}^{QM/MM} = \Omega_{AB} + \frac{\Phi_A + \Phi_B}{2}, \tag{15}$$

$$\Phi_A = \sum_M^{MM\,atoms} Q_M \frac{1}{|\vec{r}_A - \vec{R}_M|}, \tag{16}$$

where Q_M is the charge of the MM atom M and $|\vec{r}_A - \vec{R}_M|$ is the distance between the QM atom A and the MM atom M.

With that, a new set of CP-DFTB equations emerges, involving the derivatives of $c_{\mu i}$, Ω_{AB}, and Δq_A with respect to the coordinates of MM atoms, generally b. These will be evaluated in an analogous iterative procedure to that in the previous section, with several contributions vanishing.

The matrix $\mathscr{U}^{(b)}$ expresses the derivatives of MO coefficients $c_{\mu m}$ with respect to the coordinate b of an MM atom,

$$\frac{\partial c_{\mu i}}{\partial b} = \sum_m^{MO} U_{mi}^{(b)} c_{\mu m}. \tag{17}$$

Here, the diagonal elements vanish due to the vanishing derivative of overlap,

$$U_{ii}^{(b)} = -\frac{1}{2} \sum_{\mu,v}^{AO} c_{\mu i} c_{vi} \frac{\partial S_{\mu v}}{\partial b} = 0. \tag{18}$$

Due to the vanishing derivatives of $S_{\mu v}$ and $H_{\mu v}^0$, the off-diagonal elements are

$$U_{ij}^{(b)} = \frac{1}{\varepsilon_j - \varepsilon_i} \sum_{A,B}^{QM\,at.} \frac{\partial \Omega_{AB}}{\partial b} \sum_{\mu \in A} \sum_{v \in B} c_{\mu i} c_{vj} S_{\mu v}. \tag{19}$$

In addition, here, the iterative CP-DFTB-QMMM calculation may be started with the entire matrix $\mathscr{U}^{(b)}$ zeroed.

Next, the derivatives of QM charges with respect to MM coordinates are calculated from $\mathscr{U}^{(b)}$, with the first of the two contributions vanishing due to the vanishing derivatives of $S_{\mu\nu}$,

$$\frac{\partial \Delta q_A}{\partial b} = \sum_i^{MO} n_i \sum_m^{MO} U_{mi}^{(b)} \sum_{\mu \in A}^{AO} \sum_\nu (c_{\mu m} c_{\nu i} + c_{\mu i} c_{\nu m}) S_{\mu\nu}. \quad (20)$$

The iteration concludes with the calculation of derivatives of the atomic shift with respect to MM coordinates using the derivatives of QM charges. The derivatives of γ and Γ with respect to the coordinates of MM atoms vanish, leading to the following expression:

$$\begin{aligned}\frac{\partial \Omega_{AB}^{QM/MM}}{\partial b} = \sum_C^{QM\,at.} &\left(\frac{\gamma_{AC} + \gamma_{BC}}{2} + \frac{\Delta q_A \Gamma_{AC} + \Delta q_B \Gamma_{BC}}{3} \right. \\ &+ \Delta q_C \frac{\Gamma_{CA} + \Gamma_{CB}}{6} \right) \frac{\partial \Delta q_C}{\partial b} + \frac{1}{3} \sum_C^{QM\,at.} \left(\frac{\partial \Delta q_A}{\partial b} \Gamma_{AC} \right. \\ &+ \frac{\partial \Delta q_B}{\partial b} \Gamma_{BC} + (\Gamma_{CA} + \Gamma_{CB}) \frac{\partial \Delta q_C}{\partial b} \right) \Delta q_C \\ &+ \frac{1}{2} Q_M \left(\frac{xyz_A - b}{|\vec{r}_A - \vec{R}_M|^3} + \frac{xyz_B - b}{|\vec{r}_B - \vec{R}_M|^3} \right). \quad (21)\end{aligned}$$

Here, M is the MM atom of which b is one of the three Cartesian coordinates; furthermore, xyz_A is the same Cartesian coordinate of the QM atom A (x, y, and z-coordinate if b is the x, y, and z-coordinate of the MM atom M, respectively). The procedure then continues with the calculation of the matrix $\mathscr{U}^{(b)}$ according to Eq. (19).

E. Facilitating the convergence

Each of the previously described loops is iterated until the convergence of the charge derivatives has been reached. The convergence is accelerated by means of Broyden mixing[28] applied to these derivatives, similar to the application of Broyden mixing in the self-consistent-charges procedure of DFTB itself.

Practical implementation showed that the denominator $1/(\varepsilon_j - \varepsilon_i)$ makes the CP equations very numerically unstable in some cases. Especially in large molecules, the orbital energies may approach very closely accidently, leading to an expression of the type "0/0." This consequently introduces large numerical errors, and an especially difficult convergence of the CP equations. This is solved by never really forming the matrix $\mathscr{U}$ but instead by forming two equivalent matrices $\mathscr{W}$ ($W_{ij} = n_i U_{ij} + n_j U_{ji}$) and $\mathscr{V}$ ($V_{ij} = n_i \varepsilon_i U_{ij} + n_j \varepsilon_j U_{ji}$), which avoids the problem of small denominators while being formally equivalent to computing $\mathscr{U}$. Later, the charge derivatives are computed using $\mathscr{V}$ and $\mathscr{W}$.

The implementation also includes the previous developments of Nishimoto & Irle, which cover the cases of fractional occupation numbers n_i,[29] with the additional use of degenerate perturbation theory (leading to analytical behavior in the event of level crossings).[30] This leads to the modification of Eqs (11) and (12). First, by orthogonalizing degenerate eigenvectors against the perturbation

such that the relevant sub-block of U for these states becomes diagonal, and second, by introducing the finite temperature filling of the states with respect to the Fermi energy, ε_F,[31]

$$n_i(\varepsilon_i, \varepsilon_F) = \frac{1}{1 + \exp\left[\beta(\varepsilon_i - \varepsilon_F)\right]}, \quad (22)$$

into the coupled perturbed equations,

$$\tilde{U}_{ii}^{(b)} \to \tilde{\delta} \quad \text{as} \quad \varepsilon_i \to \varepsilon_F, \quad (23)$$

$$\tilde{\delta} = \frac{\beta}{2\left(1 + \cosh\left[\beta(\varepsilon_i - \varepsilon_F)\right]\right)} \tilde{U}_{ij}^{(b)} = n_i n_j U_{ij}, \quad (24)$$

where, due to orthogonalization against the perturbation, only the diagonal part of $\tilde{U}$ is non-zero between degenerate states. Additionally, to compensate for the shift of the electron chemical potential due to the perturbation, Eq. (13) is also modified due to

$$\Delta \tilde{q}_A = \Delta q_A + \sum_i \Delta q_A^i \tilde{\delta} \beta \left(\frac{\partial \varepsilon_i}{\partial b} - \frac{\partial \varepsilon_F}{\partial b} \right). \quad (25)$$

It should be noted that with the orthogonalization of states against the perturbation (i.e., the numerator becomes zero), the above-mentioned term of the type "0/0" can be safely neglected without ever evaluating $1/(\varepsilon_j - \varepsilon_i)$. For mixed derivatives where the perturbations are not simultaneously diagonalizable, the concern about stability in the previous paragraph definitely applies.

III. SIMULATION DETAILS

A. System setup

The PMFs were obtained for PCET between two tyrosine side chains (hereafter referred to as "tyrosines") in 32 different setups with various charge states, conformations, and environments (see Fig. 1. The two tyrosines either carry a negative charge (Tyr_2^- anion) or have an unpaired electron ($Tyr_2^{\bullet}$ radical) and were considered in one of two different conformations, "flipped" or "stacked." These terms refer to the configurations of $\alpha Y731 + \beta Y356$ and $\alpha Y731 + \alpha Y730$ in RNR, respectively.[5] A PCET across the α/β interface in RNR probably only occurs when $\alpha Y731$ is flipped-out and facing $\beta Y356$, whereas a PCET between $\alpha Y731$ and $\alpha Y730$ probably only occurs in a stacked configuration. Finally, the tyrosines were considered in the gas phase or in a microhydrated environment. These choices led to 32 different simulation setups, as illustrated in Fig. 1. The initial structures for the simulations were taken from QM/MM simulations[32] of RNR based on a docking model.[33]

The two obtained structures of the flipped and stacked conformations were centered in a cubic box sized $100 \times 100 \times 100$ nm^3. Next, the positions of all atoms were shifted manually to O_1–O_2 distances of $R = 2.4, 2.6, 2.8,$ or 3.0 Å, on which harmonic restraints with a force constant of 100000 kJ mol^{-1} nm^{-2} were applied. To maintain the overall conformations while leaving enough flexibility and thus variance of atomic charges during the MD simulations, spherical restraints were applied to the carbon atoms of the aromatic rings and the oxygen atoms. This allowed the atoms to move freely within a distance of 0.5 Å from their initial positions.
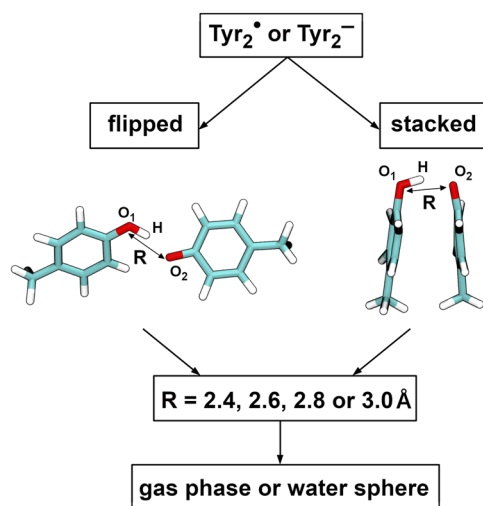
FIG. 1. Various systems used for testing the implementation of CP equations in DFTB3. The systems consist of the side chains of two tyrosines starting from Cβ with one proton removed from an oxygen atom O$_2$. Two charge states were considered, negatively charged (Tyr$_2^-$) or neutral with an unpaired electron (Tyr$_2^\bullet$), and two different conformations, flipped and stacked. In addition, the O$_1$–O$_2$ distances were restrained to R = 2.4, 2.6, 2.8, or 3.0 Å. The systems were then simulated either in the gas phase or in a sphere of water molecules, resulting in a total of 32 different setups.

Beyond that radius, a harmonic restraint with a force constant of 100000 kJ mol^{-1} nm^{-2} was set in and pulled the atoms back into the sphere. Additional harmonic restraints with a force constant of 1000 kJ mol^{-1} nm^{-2} were applied to the sum of O$_1$H and O$_2$H distances, when $|$O$_1$H$| + |$O$_2$H$| > (R + 0.2$ Å$)$, to favor the hydrogen bonded configurations.

Finally, the 16 generated setups were duplicated for two different sets of simulations. In the first set, the tyrosines were kept in the gas phase. In the second set, a solvation shell of water molecules was formed around the molecules. Both sets of simulations were performed with a local version of GROMACS 2020[34–37] patched with a local version of PLUMED 2.5.1[38–40] and interfaced with DFTB+ 19.1[41,42] including the aforementioned implementation of CP-DFTB equations[21,27,43] for DFTB3.

B. Simulations in the gas phase

The gas-phase systems were described solely with DFTB3 using the 3OB parameter set. They were equilibrated for 1 ns using the leap-frog integrator with a time step of 0.5 fs. Subsequently, multiple walker metadynamics simulations[44,45] of the PCET were performed using two collective variables.

The first CV is the difference of O–H distances

$$\Delta d = |\text{O}_1\text{H}| - |\text{O}_2\text{H}| \qquad (26)$$

to describe the proton transfer process, and the other CV, the difference of the total charge of each tyrosine (excluding the hydrogen atom being transferred),

$$\Delta Q = \underbrace{\sum_i^{\text{mol \#1}} \Delta q_i}_{Q_1} - \underbrace{\sum_j^{\text{mol \#2}} \Delta q_j}_{Q_2}, \qquad (27)$$

describes the electron transfer process; Δq_i and Δq_j are the Mulliken charges of atoms belonging to the first and second tyrosine, respectively.

All gas-phase simulations used 16 walkers in which Gaussian biasing potentials were added every 500 steps with a height of 0.5 kJ mol^{-1} and a width of 0.05 Å for the first CV and 0.02 e for the second CV. The bias between walkers was exchanged every 500 steps. All Tyr$_2^-$ systems used a time step of 0.5 fs, and each of the eight setups yielded a total simulation time of 2 ns. For the Tyr$_2^\bullet$ systems, the time step was increased to 1 fs, and each setup yielded a total simulation time of at least 11.2 ns and up to 16.5 ns.

C. Simulation in aqueous solution

For the simulations in aqueous solution, 35 water molecules were placed around the flipped conformations, and 30 water molecules were placed around the stacked conformations such that a solvation shell was formed. The simulations were performed in a QM/MM approach, i.e., the tyrosines were described with DFTB3 using the 3OB parameter set, while the water molecules were represented with the MM model TIP3P.[46] The Lennard–Jones parameters from the AMBER99 force field[47] were considered for the atoms in the QM region (note: these are unchanged in the refined force fields AMBER99SB and AMBER99SB-ILDN). To keep the water molecules in place, spherical restraints were applied to the oxygen atoms, i.e., after moving further away than 1 Å from their initial positions, harmonic restraints with a force constant of 100000 kJ mol^{-1} nm^{-2} were set in, pushing the atoms back.

Analogously to the simulations in the gas phase, the solvated tyrosine systems were equilibrated for 1 ns with a time step of 0.5 fs. The electrostatic and van der Waals interactions in the MM region and between the QM and MM regions were cut off at 2 nm. Next, metadynamics simulations were performed with the previously introduced set of reaction coordinates, Δd and ΔQ, using the same Gaussian heights, widths, deposition rates, and bias exchange strides. However, the time step was set to 1 fs for all simulations, and 24 walkers were used in each setup. The flipped and stacked Tyr$_2^-$ systems yielded a total simulation time of 2.2, 3.2, 4, and 7 ns for R = 2.4, 2.6, 2.8, and 3.0 Å, respectively. The flipped Tyr$_2^\bullet$ systems yielded a total simulation time of 3.9, 13.3, 9.5, and 4.2 ns for 2.4, 2.6, 2.8, and 3.0 Å, respectively. The stacked Tyr$_2^\bullet$ systems yielded a total simulation time of 9.2, 7.8, 9.4, and 6.8 ns for R = 2.4, 2.6, 2.8, and 3.0 Å, respectively.

IV. RESULTS AND DISCUSSION

The resulting two-dimensional PMFs of the PCET processes are presented and discussed below. In all cases, a negative Δd corresponds to the O$_1$–H bond being in place, while a positive Δd means that O$_2$ and H are bonded. The range of available values of ΔQ differs between the two kinds of systems.

In the anionic Tyr$_2^-$ systems, the H atom carries a partial charge of about 0.4 e. When it is bonded to O$_1$, then $Q_1 \approx -0.4$ e. Tyrosine no. 2 carries the negative charge; therefore, $Q_2 \approx -1.0$ e,

Anionic System
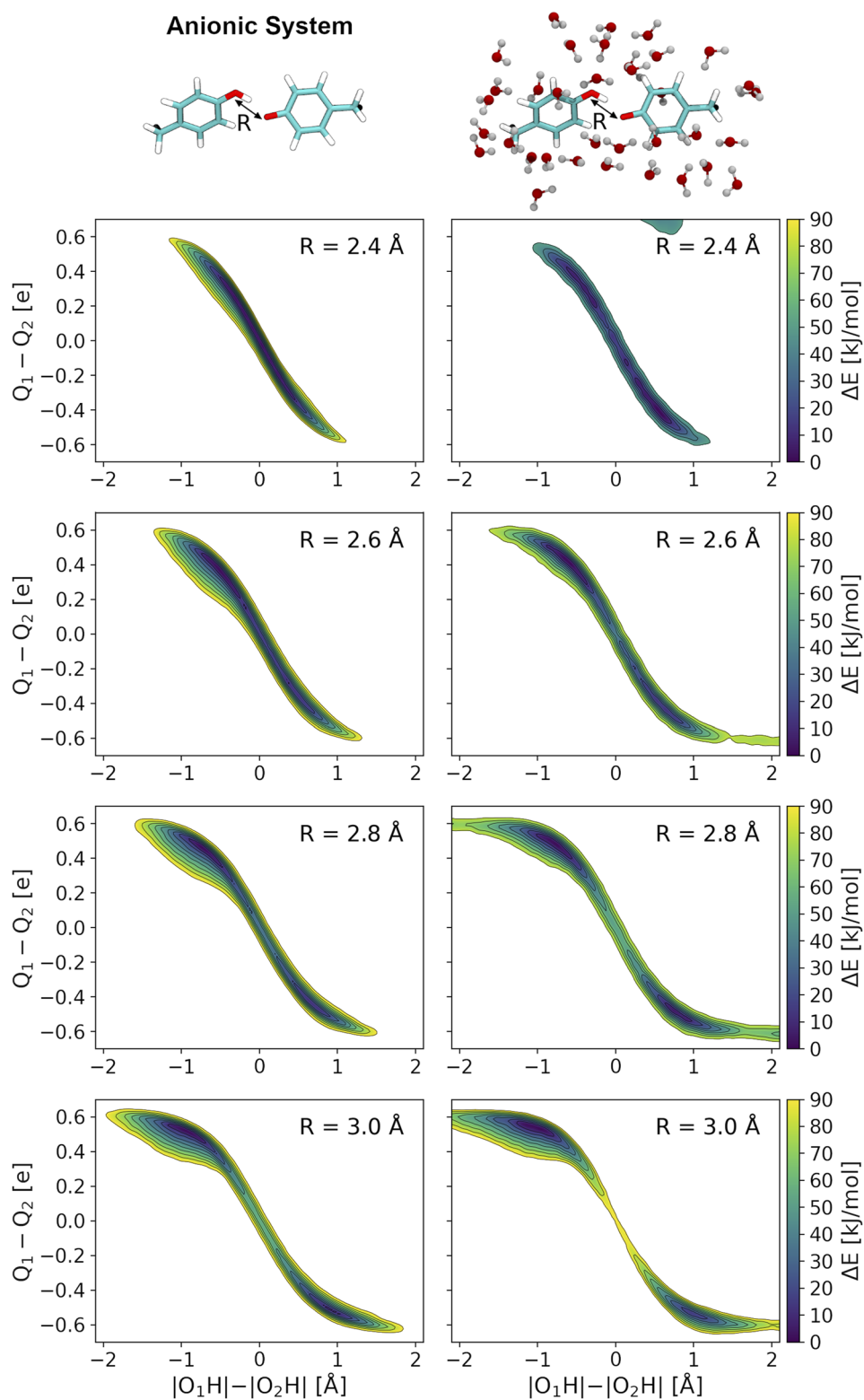
FIG. 2. Potentials of the mean force of PCET reactions in the flipped Tyr$_2^-$ conformation in the gas phase (left) or in a sphere of water molecules (right) for different O$_1$–O$_2$ distances of R = 2.4, 2.6, 2.8, and 3.0 Å (top to bottom). The horizontal axis represents the PT coordinate, and the vertical axis represents the ET coordinate. Contour lines are drawn every 10 kJ/mol.
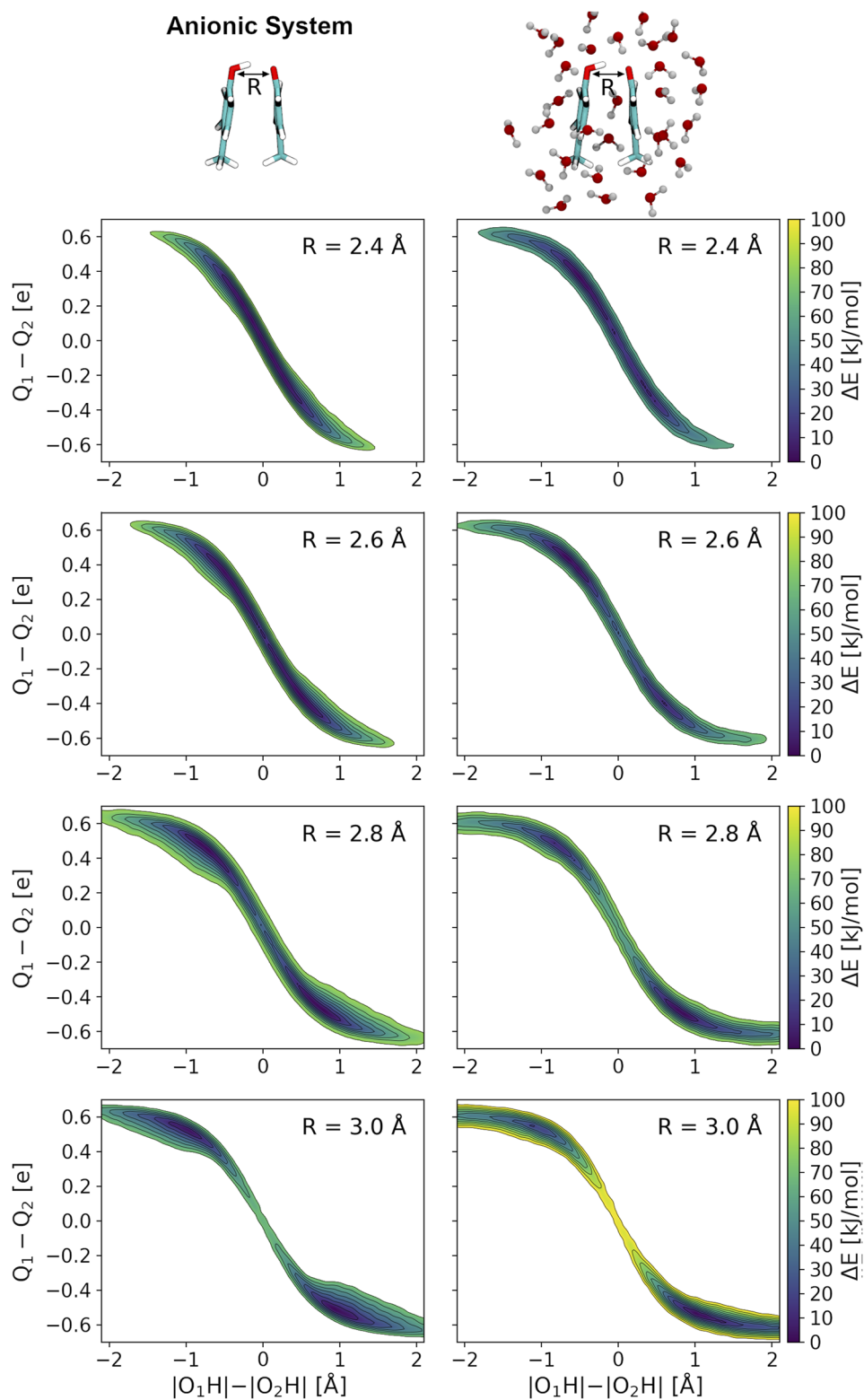
FIG. 3. Potentials of the mean force of PCET reactions in the stacked Tyr$_2^-$ conformation in the gas phase (left) or in a sphere of water molecules (right) for different O$_1$–O$_2$ distances of R = 2.4, 2.6, 2.8, and 3.0 Å (top to bottom). The horizontal axis represents the PT coordinate, and the vertical axis represents the ET coordinate. Contour lines are drawn every 10 kJ/mol.

and consequently, $\Delta Q = 0.6$ e. Similarly, $\Delta Q = -0.6$ e whenever the hydrogen is bonded to tyrosine no. 2.

In the radical $Tyr_2^{\bullet}$ systems, the hydrogen atom being transferred carries a charge of ~ 0.2 e, and whenever it is bonded to tyrosine no. 1, the sum of the atomic partial charges of tyrosine no. 1 is ca. -0.2 e. Since the system is electroneutral, the total charge of tyrosine no. 2 is ~ 0.0 e. Consequently, $\Delta Q = -0.2$ e whenever the hydrogen is bonded to O_2, and when $\Delta Q = 0.2$ e, the $H-O_1$ bond is in place.

A. Anionic systems

The two-dimensional PMFs of the PCET in the Tyr_2^{-} systems in the flipped and stacked conformations are shown in Figs. 2 and 3. Qualitatively, they all appear almost the same, except for the gas-phase simulations with $R = 2.4$ Å. In these two simulations, there is one narrow minimum around $\Delta d = 0$ and $\Delta Q = 0$, which corresponds to a shared proton between O_1 and O_2. In all other simulations, there are two narrow minima corresponding to the O_1-H and O_2-H bonds. The minima should be of equal depth, which is the case for most of the simulations but not all. This can be attributed to a lack of convergence, which could be improved by extending the simulations or passing to the well-tempered variant of metadynamics.[48] Nonetheless, all simulations ran without any problems and showed the expected behavior, such as an increase in the barrier height with increasing $|O_1-O_2|$ distances. The obtained transition state energies are plotted in Fig. 4 and listed in Table I.

As mentioned previously, the gas-phase simulations in the flipped and stacked conformations for $R = 2.4$ Å share the hydrogen atom; thus, there is no barrier. At larger distances, the proton is no longer shared, and the height of the barriers increases with the O_1-O_2 distances. In the gas phase, the transition state energy in the stacked conformation is 6 and 3 kJ/mol lower than that in the flipped conformation at intermediate distances of $R = 2.6$ and 2.8 Å. At $R = 3.0$ Å, however, the barrier is 12 kJ/mol higher in the stacked conformation.
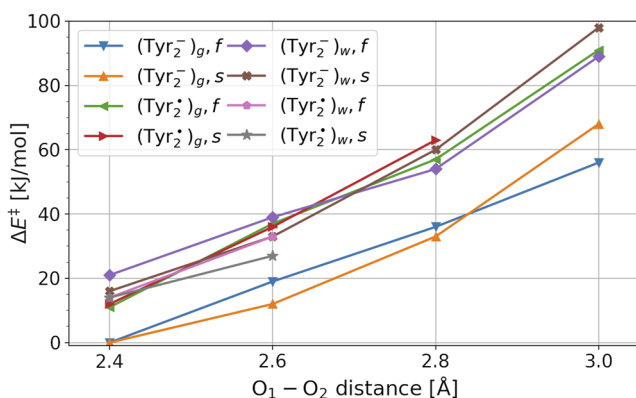
FIG. 4. Reaction barriers of proton-coupled electron transfers performed in gas phase (subscript g) and a sphere of water (subscript w) in the flipped (f) and stacked (s) conformations. Missing values correspond to unconverged simulations where no energy barrier could be determined.

TABLE I. Reaction barriers of proton-coupled electron transfers for the Tyr_2^{-} and $Tyr_2^{\bullet}$ systems performed in the gas phase (subscript g) and a sphere of water (subscript w) in the flipped (f) and stacked (s) conformations. Energies are given in kJ/mol. Missing values correspond to unconverged simulations where no energy barrier could be determined.

Setup	2.4 Å	2.6 Å	2.8 Å	3.0 Å
$(Tyr_2^{-})_g$, f	0	19	36	56
$(Tyr_2^{-})_g$, s	0	12	33	68
$(Tyr_2^{-})_w$, f	21	39	54	89
$(Tyr_2^{-})_w$, s	16	33	60	98
$(Tyr_2^{\bullet})_g$, f	11	37	57	91
$(Tyr_2^{\bullet})_g$, s	12	36	63	
$(Tyr_2^{\bullet})_w$, f	14	33		
$(Tyr_2^{\bullet})_w$, s	14	27		

The reaction barriers increase significantly when the systems are solvated in a sphere of MM water. For $R = 2.4$ Å, the proton is no longer shared between O_1 and O_2 but rather bonded to either one of them. For a PCET, a barrier of 21 and 16 kJ/mol has to be overcome in the flipped and stacked conformations, respectively. At $|O_1-O_2| = 2.6$ Å, the barrier heights are 39 and 33 kJ/mol, respectively. Hence, a PCET occurs more likely at short O_1-O_2 distances when the tyrosines are stacked. By contrast, at larger O_1-O_2 distances of 2.8 and 3.0 Å, the barrier heights in the flipped conformations are lower by 6 and 9 kJ/mol than those in the stacked conformation, respectively.

It should be noted that for comparable O_1-O_2 distances, the reaction barriers obtained here are higher than those obtained in our preceding work.[19] A likely explanation is that the tyrosines were restrained in Ref. 19 to a smaller extent than in the current work, which led to larger fluctuations toward shorter O_1-O_2 distances and consequently smaller barriers.

Also, the metadynamics simulations of the flipped system in a water sphere with $R = 2.4$ Å resolved an additional, higher-energy region, visible at the top of the plot. The CV values of this area correspond to tyrosine no. 1 being a deprotonated radical, while protonated tyrosine no. 2 carries the additional electron ($Tyr_1-O^{\bullet} \ldots Tyr_2-OH^{-}$). This state of the system seems to be less stable than the "usual" state in which the deprotonated tyrosine carries the negative charge, as also illustrated by the higher free energy of this state of 32 kJ/mol.

B. Radical systems

The two-dimensional PMFs of the PCET reactions in the $Tyr_2^{\bullet}$ systems are shown in Figs. 5 and 6. The incomplete convergence of some of the simulations was caused by the low-energy basins on the PMF being much broader than in the anionic systems described previously. Clearly, larger numbers of Gaussian biasing potentials are needed to fill the basins, compared to the narrow PMFs in the Tyr_2^{-} systems. Hence, especially the simulations of the hydrated systems at O_1-O_2 distances of 2.8 and 3.0 Å would require extension in order to reach convergence, as would the gas-phase simulation with $R = 3.0$ Å in the stacked conformation.

The converged simulations in the gas phase exhibit two broad minima of equal depth, corresponding to the O_1-H and O_2-H
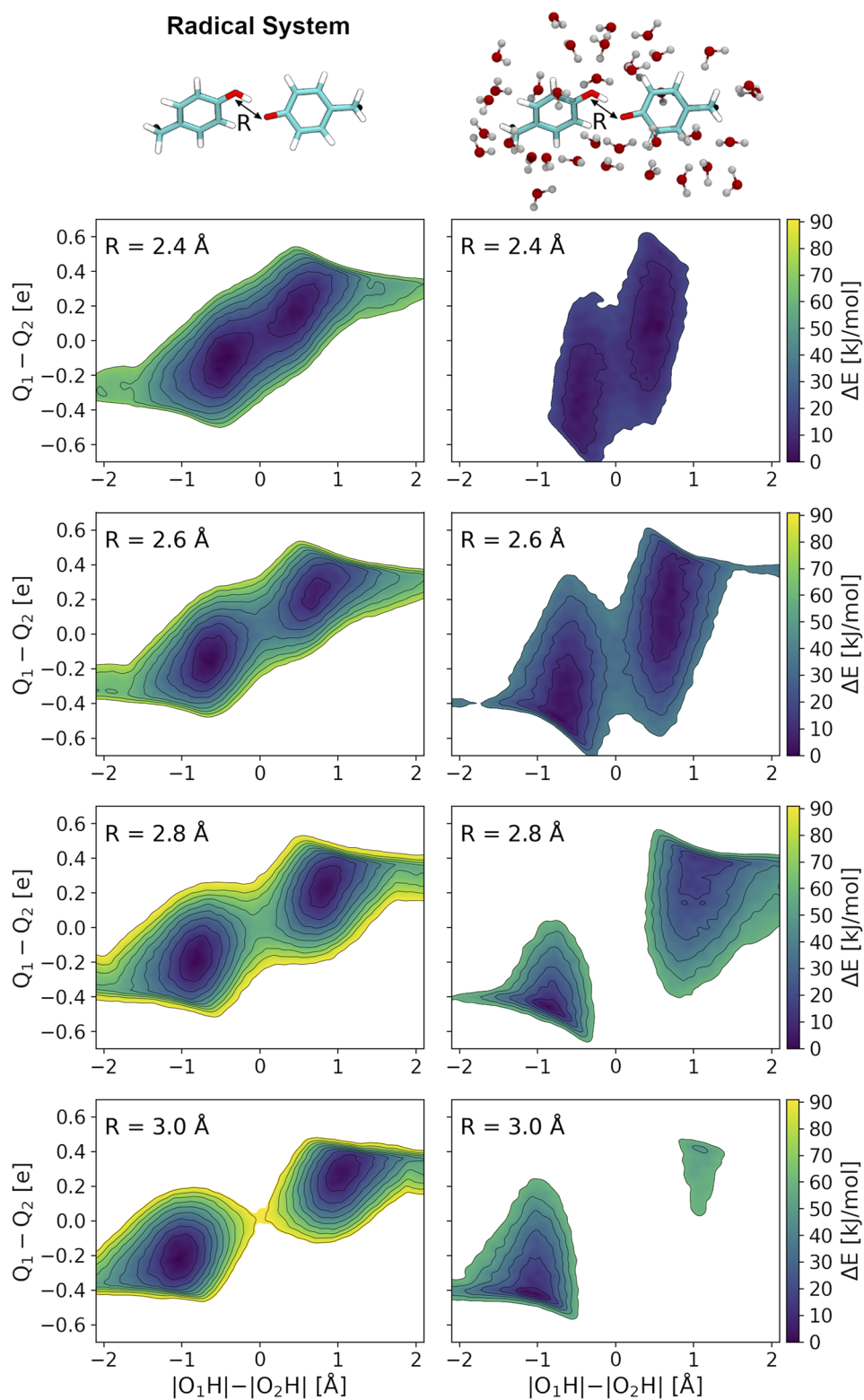
FIG. 5. Potentials of the mean force of PCET reactions in the flipped $Tyr_2^\bullet$ conformation in the gas phase (left) or in a sphere of water molecules (right) for different O_1–O_2 distances of $R = 2.4$, 2.6, 2.8, and 3.0 Å (top to bottom). The horizontal axis represents the PT coordinate, and the vertical axis represents the ET coordinate. Contour lines are drawn every 10 kJ/mol.
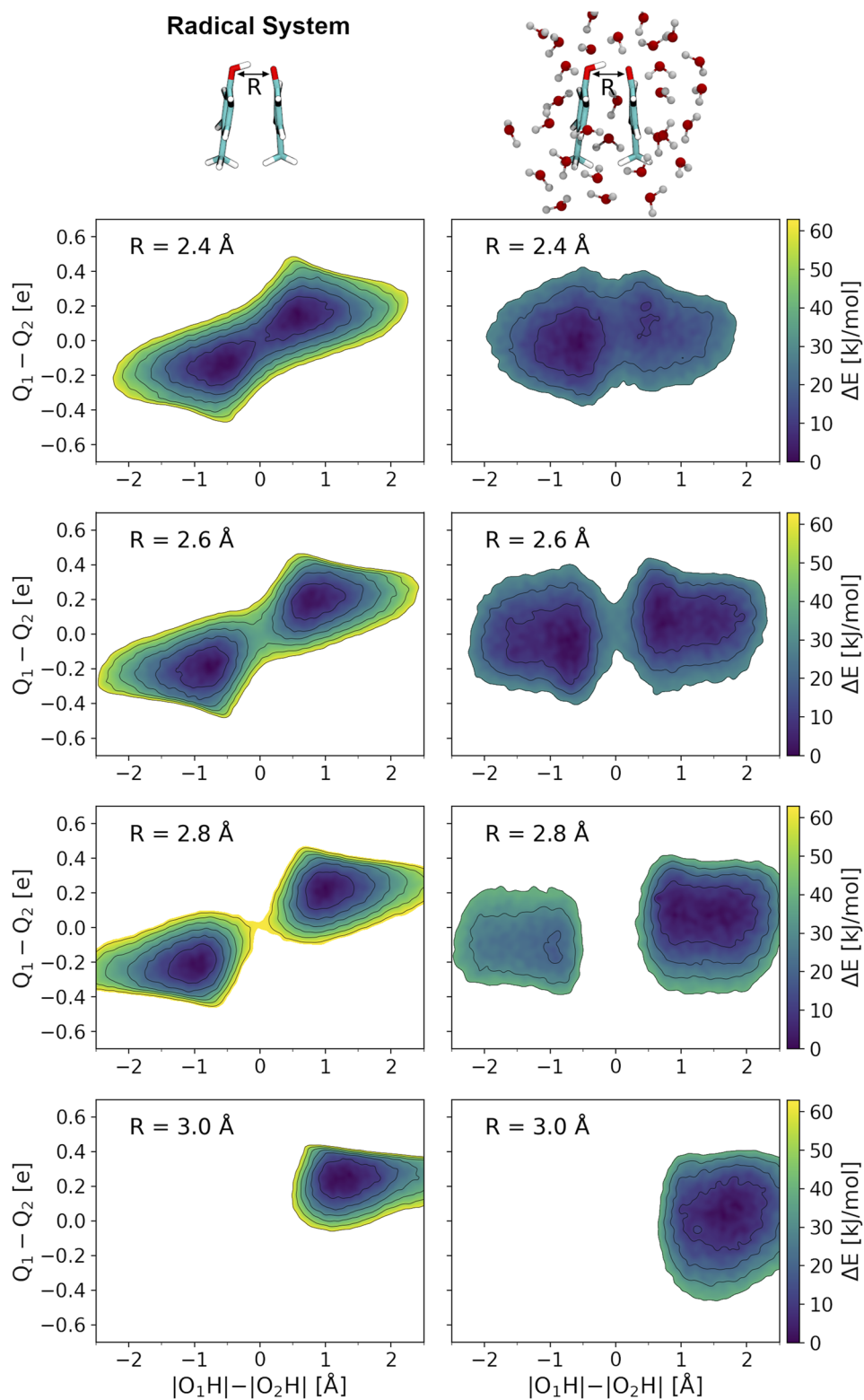
FIG. 6. Potentials of the mean force of PCET reactions in the stacked Tyr$_2$$^\bullet$ conformation in the gas phase (left) or in a sphere of water molecules (right) for different O$_1$–O$_2$ distances of R = 2.4, 2.6, 2.8, and 3.0 Å (top to bottom). The horizontal axis represents the PT coordinate, and the vertical axis represents the ET coordinate. Contour lines are drawn every 10 kJ/mol.

bonds. At short O_1–O_2 distances of 2.4 and 2.6 Å, the barrier heights for a PCET are 11 and 37 kJ/mol (in the flipped conformation) and 12 and 36 kJ/mol (in the stacked conformation), so they are actually the same in the two different structures. At R = 2.8 Å, the barrier of 57 kJ/mol in the flipped conformation is 6 kJ/mol smaller than that in the stacked conformation. Since the metadynamics simulation of the stacked conformation at R = 3.0 Å did not converge, the barrier heights cannot be compared for this O_1–O_2 distance.

Several interesting things happen when the tyrosines are embedded in a sphere of water molecules. The reaction barriers do not increase significantly for R = 2.4 Å, only by 3 and 2 kJ/mol in the flipped and stacked conformations, respectively. At R = 2.6 Å, the heights of the barriers even decrease by 8 and 9 kJ/mol. Moreover, the topography of the PMF changes compared to the gas phase simulations.

In the flipped conformation with R = 2.4 Å, the two minima are broader in the direction of the ET coordinate. This effect disappears at longer O_1–O_2 distances of 2.6, 2.8, and 3.0 Å to a large extent. Although the simulations with the water sphere at R = 2.8 and 3.0 Å did not converge completely, the low-energy basins appear markedly isolated, leading to the expectation that the barrier to transfer will be considerably higher than in the gas phase.

In the stacked conformation, the minima are slightly broader than in the gas phase simulations. They are shifted closer to ΔQ = 0 e, i.e., the sum of the partial charges is nearly the same in tyrosine nos 1 and 2, although the charge difference appears to increase somewhat as the O_1–O_2 distance increases. Still, a definite statement can only be made as soon as the simulations for R = 2.8 and 3.0 Å have converged, which is not the case yet. The slow convergence of those simulations also makes it difficult to compare the barrier heights to the flipped systems; although the basins appear physically closer to each other so that lower barriers would be expected potentially, this cannot be said for sure at this stage. The minima for R = 2.4 Å are not equally deep, due to a nearby water molecule forming a hydrogen bond with O_2 and therefore stabilizing the deprotonated state of tyrosine no. 2.

The change of charge between the reactant and product appears small, especially in the hydrated radical systems. This means that the ET coordinate based on the difference of charges, Q_1–Q_2, seems to be reaching the limits of its applicability in these radical complexes. A simple and practicable solution to this issue may be to define the charges Q_1 and Q_2 for subsets of atoms rather than the entire fragment such that the difference Q_1–Q_2 increases for the reactant and the product. A more systematic solution may be to implement a spin-polarized DFTB model,[49,50] which would make it possible to access spin populations on the participating molecular fragments and likely be a useful tool to characterize radical systems. This remains beyond the scope of the current work.

C. Computational cost

The average timings presented in the following are taken from short, unbiased QM and QM/MM simulations performed on a single core of the Intel Xeon Silver 4214 CPU. We find a significant increase in the computational cost associated with the solution of CP-DFTB equations. For the anionic Tyr_2^- systems, one MD step in the gas phase takes 2.18 s. Only 1.6% accounts for the self-consistent-charge DFTB3 calculation and 98.3% for the solution of

the CP-DFTB equations, which is a 59-fold increase. An MD step of the $Tyr_2^\bullet$ system in the gas phase takes 5.18 s, where the DFTB3 calculation takes 1.1% of the time and the CP-DFTB calculation takes the remaining 98.9%. Consequently, the cost is increased by a factor of 90.

When the systems are solvated in a sphere of water, the computational cost increases even more because of the additional derivatives with respect to the coordinates of the MM atoms. An MD step of the Tyr_2^- systems takes 6.71 s, of which 0.55% is spent in the DFTB3 calculation and 99.45% is accounted for in the solution of the CP-DFTB equations (a 180-fold increase). For the $Tyr_2^\bullet$ systems, one step takes 15.08 s, where 0.3% accounts for DFTB3 and the remaining 99.7% for the solution of the CP-DFTB equations (a 333-fold increase).

The observed substantial computational cost of the solution of CP-DFTB equations makes it clear that the application of the method to realistic biophysical problems would greatly benefit from further optimization or approximation. As mentioned in Ref. 19 already, since the calculation of derivatives with respect to the coordinates of different (QM or MM) atoms is entirely independent of each other, the simplest kind of optimization would be a trivial parallelization, for example, with OpenMP.

In order to apply the QM/MM CP-DFTB approach to realistic biomolecular complexes, it will be necessary to introduce additional approximations. The first idea would be a simple cut-off, meaning that the derivatives of QM atomic charges would only be evaluated with respect to the coordinates of those MM atoms that are within a certain distance of the QM region. The applicability and numerical accuracy of such an approximation are yet to be established. A potentially more promising way might be to identify a component of the CP equations that contributes relatively little at longer distances and, at the same time, either takes long to calculate or increases the number of CP iterations necessary. That component, rather than the entire charge derivative, might then be neglected beyond a certain cut-off distance. Still, the dependence of the presented model on cut-off parameters and algorithmic simplifications needs to be tested carefully because the associated parameter dependences might not be readily obvious.

V. CONCLUSION AND OUTLOOK

We implemented CP equations into DFTB3 as an extension to the previous work by Gillet et al.,[19] where biasing potentials were applied to partial atomic charges in extended sampling MD simulations. The gradients of the potentials are calculated by solving the CP-DFTB equations, which were originally developed in the context of DFTB by Witek et al.[21] The previous scheme worked well for pure QM systems; however, hybrid QM/MM simulations were unstable and failed to converge because the derivatives of QM atomic charges with respect to MM atomic coordinates were missing. Based on an earlier development by Hourahine,[27] we implemented the missing gradients. The implementation described here is available for download from our local fork of the DFTB+ source code deposited at GitHub.[43]

In order to test the new framework, we performed 32 metadynamics simulations of PCETs in a small test system. The systems differed in their charge states and conformations. In addition, the systems were either simulated in the gas phase in a QM setup or in

a sphere of water molecules in a QM/MM setup. We considered two reaction coordinates, one for the ET process composed of Mulliken atomic charges as introduced in our previous work and one for the PT process.

All QM and QM/MM simulations were stable, and most of the simulations converged well when simulated long enough. An exception is the simulation of radical systems with long O_1–O_2 distances, which require an extremely large area of configuration space to be covered and also exhibit a very high energy barrier. In all of the other systems, the minima of free energy were correctly identified, and meaningful transition state energies were obtained. The only drawback was the computational cost that increased substantially due to the CP equations. Nonetheless, the implementation of CP-DFTB equations and the additional gradients were successful. The scheme may be used in more complex molecular systems, for example, PCET reactions involving more than two molecules or a PCET reaction in a protein environment. Such an application will require additional optimizations and possible approximations.

AUTHOR DECLARATIONS

Conflict of Interest

The authors have no conflicts to disclose.

Author Contributions

Denis Maag: Investigation (equal); Validation (equal); Visualization (equal); Writing – original draft (equal). **Josua Böser**: Investigation (equal); Visualization (equal). **Henryk A. Witek**: Conceptualization (equal); Methodology (equal); Software (equal); Writing – original draft (equal). **Ben Hourahine**: Methodology (equal); Software (equal); Writing – original draft (equal). **Marcus Elstner**: Funding acquisition (equal); Supervision (equal). **Tomáš Kubař**: Conceptualization (equal); Funding acquisition (equal); Methodology (equal); Software (equal); Supervision (equal); Writing – original draft (equal).

DATA AVAILABILITY

The data that support the findings of this study are available from the corresponding author upon reasonable request.

REFERENCES

[1] J. M. Mayer, Annu. Rev. Phys. Chem. **55**, 363 (2004).
[2] S. Hammes-Schiffer, Energy Environ. Sci. **5**, 7696 (2012).
[3] J. Stubbe, D. G. Nocera, C. S. Yee, and M. C. Y. Chang, Chem. Rev. **103**, 2167 (2003).
[4] E. C. Minnihan, D. G. Nocera, and J. Stubbe, Acc. Chem. Res. **46**, 2524 (2013).
[5] C. R. Reinhardt, P. Li, G. Kang, J. Stubbe, C. L. Drennan, and S. Hammes-Schiffer, J. Am. Chem. Soc. **142**, 13768 (2020).
[6] R. I. Cukier, J. Phys. Chem. **98**, 2377 (1994).
[7] R. I. Cukier, J. Phys. Chem. **99**, 16101 (1995).
[8] R. I. Cukier, J. Phys. Chem. **100**, 15428 (1996).
[9] A. Soudackov and S. Hammes-Schiffer, J. Chem. Phys. **111**, 4672 (1999).
[10] A. Soudackov and S. Hammes-Schiffer, J. Chem. Phys. **113**, 2385 (2000).
[11] H. Decornez and S. Hammes-Schiffer, J. Phys. Chem. A **104**, 9370 (2000).
[12] M. H. V. Huynh and T. J. Meyer, Chem. Rev. **107**, 5004 (2007).
[13] V. R. I. Kaila, M. I. Verkhovsky, and M. Wikström, Chem. Rev. **110**, 7062 (2010).
[14] D. R. Weinberg, C. J. Gagliardi, J. F. Hull, C. F. Murphy, C. A. Kent, B. C. Westlake, A. Paul, D. H. Ess, D. G. McCafferty, and T. J. Meyer, Chem. Rev. **112**, 4016 (2012).
[15] A. Migliore, N. F. Polizzi, M. J. Therien, and D. N. Beratan, Chem. Rev. **114**, 3381 (2014).
[16] N. Elgrishi, B. D. McCarthy, E. S. Rountree, and J. L. Dempsey, ACS Catal. **6**, 3644 (2016).
[17] R. Tyburski, T. Liu, S. D. Glover, and L. Hammarström, J. Am. Chem. Soc. **143**, 560 (2021).
[18] S. E. Brown and F. A. Shakib, Phys. Chem. Chem. Phys. **23**, 2535 (2021).
[19] N. Gillet, M. Elstner, and T. Kubař, J. Chem. Phys. **149**, 072328 (2018).
[20] R. S. Mulliken, J. Chem. Phys. **23**, 1833 (1955).
[21] H. A. Witek, S. Irle, and K. Morokuma, J. Phys. Chem. **121**, 5163 (2004).
[22] D. Porezag, T. Frauenheim, T. Köhler, G. Seifert, and R. Kaschner, Phys. Rev. B **51**, 12947 (1995).
[23] G. Seifert, D. Porezag, and T. Frauenheim, Int. J. Quantum Chem. **58**, 185 (1996).
[24] M. Elstner, D. Porezag, G. Jungnickel, J. Elsner, M. Haugk, T. Frauenheim, S. Suhai, and G. Seifert, Phys. Rev. B **58**, 7260 (1998).
[25] Y. Yang, H. Yu, D. York, Q. Cui, and M. Elstner, J. Phys. Chem. A **111**, 10861 (2007).
[26] M. Gaus, Q. Cui, and M. Elstner, J. Chem. Theory Comput. **7**, 931 (2011).
[27] B. Hourahine, "Modified version of the DFTB+: General package for performing fast atomistic calculations" (2021) https://github.com/bhourahine/dftbplus/tree/perturb_dx; accessed 30 December 2021.
[28] C. G. Broyden, Math. Comput. **19**, 577 (1965).
[29] Y. Nishimoto and S. Irle, Chem. Phys. Lett. **667**, 317 (2017).
[30] D. J. Griffiths, *Introduction to Quantum Mechanics*, 2nd ed. (Prentice-Hall, 1995).
[31] S. Baroni, S. de Gironcoli, A. Dal Corso, and P. Giannozzi, Rev. Mod. Phys. **73**, 515 (2001).
[32] D. Maag, "QM/MM studies of proton-coupled electron transfer in ribonucleotide reductase," Master's thesis, Karlsruhe Institute of Technology, 2018.
[33] U. Uhlin and H. Eklund, Nature **370**, 533 (1994).
[34] D. van der Spoel, E. Lindahl, B. Hess, G. Groenhof, A. E. Mark, and H. J. C. Berendsen, J. Comput. Chem. **26**, 1701 (2005).
[35] B. Hess, C. Kutzner, D. van der Spoel, and E. Lindahl, J. Chem. Theory Comput. **4**, 435 (2008).
[36] M. J. Abraham, T. Murtola, R. Schulz, S. Páll, J. C. Smith, B. Hess, and E. Lindahl, SoftwareX **1-2**, 19 (2015).
[37] T. Kubař, https://github.com/tomaskubar/gromacs-dftbplus (2022) (Last accessed September 28, 2022).
[38] G. A. Tribello, M. Bonomi, D. Branduardi, C. Camilloni, and G. Bussi, Comput. Phys. Commun. **185**, 604 (2014).
[39] M. Bonomi, G. Bussi, C. Camilloni, G. A. Tribello, P. Banáš, A. Barducci, M. Bernetti, P. G. Bolhuis, S. Bottaro, D. Branduardi, R. Capelli, P. Carloni,

M. Ceriotti, A. Cesari, H. Chen, W. Chen, F. Colizzi, S. De, M. De La Pierre, D. Donadio, V. Drobot, B. Ensing, A. L. Ferguson, M. Filizola, J. S. Fraser, H. Fu, P. Gasparotto, F. L. Gervasio, F. Giberti, A. Gil-Ley, T. Giorgino, G. T. Heller, G. M. Hocky, M. Iannuzzi, M. Invernizzi, K. E. Jelfs, A. Jussupow, E. Kirilin, A. Laio, V. Limongelli, K. Lindorff-Larsen, T. Löhr, F. Marinelli, L. Martin-Samos, M. Masetti, R. Meyer, A. Michaelides, C. Molteni, T. Morishita, M. Nava, C. Paissoni, E. Papaleo, M. Parrinello, J. Pfaendtner, P. Piaggi, G. Piccini, A. Pietropaolo, F. Pietrucci, S. Pipolo, D. Provasi, D. Quigley, P. Raiteri, S. Raniolo, J. Rydzewski, M. Salvalaglio, G. C. Sosso, V. Spiwok, J. Šponer, D. W. H. Swenson, P. Tiwary, O. Valsson, M. Vendruscolo, G. A. Voth, A. White, and The PLUMED consortium, Nat. Methods **16**, 670 (2019).

[40] T. Kubař, https://github.com/tomaskubar/plumed2/tree/v2.7 (2022) (Last accessed September 28, 2022).

[41] B. Aradi, B. Hourahine, and T. Frauenheim, J. Phys. Chem. A **111**, 5678 (2007).

[42] B. Hourahine, B. Aradi, V. Blum, F. Bonafé, A. Buccheri, C. Camacho, C. Cevallos, M. Y. Deshaye, T. Dumitrică, A. Dominguez, S. Ehlert, M. Elstner, T. van der Heide, J. Hermann, S. Irle, J. J. Kranz, C. Köhler, T. Kowalczyk, T. Kubař, I. S. Lee, V. Lutsker, R. J. Maurer, S. K. Min, I. Mitchell, C. Negre, T. A. Niehaus,

A. M. N. Niklasson, A. J. Page, A. Pecchia, G. Penazzi, M. P. Persson, J. Řezáč, C. G. Sánchez, M. Sternberg, M. Stöhr, F. Stuckenberg, A. Tkatchenko, V. W.-z. Yu, and T. Frauenheim, J. Chem. Phys. **152**, 124101 (2020).

[43] T. Kubař, https://github.com/tomaskubar/dftbplus/tree/coupled-perturb (2022) (Last accessed September 28, 2022).

[44] A. Laio and M. Parrinello, Proc. Natl. Acad. Sci. U. S. A. **99**, 12562 (2002).

[45] P. Raiteri, A. Laio, F. L. Gervasio, C. Micheletti, and M. Parrinello, J. Phys. Chem. B **110**, 3533 (2006).

[46] W. L. Jorgensen, J. Chandrasekhar, J. D. Madura, R. W. Impey, and M. L. Klein, J. Chem. Phys. **79**, 926 (1983).

[47] V. Hornak, R. Abel, A. Okur, B. Strockbine, A. Roitberg, and C. Simmerling, Proteins: Struct., Funct., Bioinf. **65**, 712 (2006).

[48] A. Barducci, G. Bussi, and M. Parrinello, Phys. Rev. Lett. **100**, 020603 (2008).

[49] C. Köhler, G. Seifert, U. Gerstmann, M. Elstner, H. Overhof, and T. Frauenheim, Phys. Chem. Chem. Phys. **3**, 5109 (2001).

[50] P. Melix, A. F. Oliveira, R. Rüger, and T. Heine, Theor. Chem. Acc. **135**, 232 (2016).